THE ANGULAR DISTRIBUTION OF SINGLE CRYSTAL MOLYBDENUM

JOSEPH BEHLER GREEN, JR.

The Angular Distribution of Single Crystal Molybdenum Sputtered by 1-10 keV Cesium Ions

By

Joseph Behler Green, Jr.

B.S. (United States Naval Academy) 1954

THESIS

Submitted in partial satisfaction of the requirements for the degree of

MASTER OF SCIENCE

in

Engineering

in the

GRADUATE DIVISION

of the

UNIVERSITY OF CALIFORNIA, BERKELEY

ABSTRACT

Yield and angular distribution measurements of sputtered molybdenum by a 1-10 kev cesium ion beam parallel to the ⟨100⟩ crystallographic direction have successfully been made employing a radioactive tracer technique previously developed for similar work done with copper. The yield was found to be dependent not only upon the incident ion energy, but also upon the target temperature. The temperature dependence was attributed to annealing out of defects created near the surface of the crystal during ion bombardment. Nonlinear regression analysis of the data indicates that most of the emitted particles were in a cosine distribution. The data showed that focusing chains are of secondary consideration in the energy and temperature regions investigated.

ACKNOWLEDGMENTS

The author would like to express his sincere appreciation to Professor Harold P. Smith, Jr., for his continuous advice and guidance which were very necessary to the completion of this study. Gratitude is due to Professors Hans M. Mark and Frank C. Hurlbut, the other two members of the thesis committee. Special thanks go to N. Thomas Olson for assistance during the experimental portion of the work and to Betty J. Dial for carefully typing the final manuscript.

TABLE OF CONTENTS

INTRODUCTION

Sputtering, or ion erosion, of surfaces has been observed for many years. There is evidence which dates initial observations as early as 1850.[1] Despite the fact that the process has been observed for over one hundred years, most of the work and, consequently, the advances in this field have been made in the last decade.

There have been many theories as to the actual mechanism of sputtering, the most recent of which was observed by Wehner[2] and explained by Silsbee.[3] This theory was based on the existence of a momentum transfer between the ion entering a crystal and the crystal atoms. If the amount of momentum transferred to the crystal atoms were great enough, surface atoms could then be ejected from the lattice structure. Silsbee proposed that in a well ordered single crystal the momentum transfer would be along the crystallographic directions of the target material. Consequently, he surmised that, since the close packed direction could effect this momentum transfer most easily, there should be preferential sputtering characteristic of the close packed direction.

Work was begun at the University of California in 1963 by Smith and Olson[4] to verify experimentally this preferential sputtering, or focusing effect, of the close packed Silsbee chains. The research was carried out using monocrystalline copper as the target material and Cs^{137} ions (singly ionized) as the bombarding ions. The complete results of this experimentation can be found in the Ph.D. thesis of Olson.[4] Briefly, Olson and Smith found that focusing of the close packed chains

did exist although it was a small effect. They observed that the majority of the sputtered particles were attributed to random scattering from atoms near the crystal surface where there was a large energy transfer.

Upon completion of this work, it was decided to employ the technique and equipment developed by Olson to investigate molybdenum sputtering. It is the purpose of this thesis to report the results using molybdenum as the target material sputtered by cesium ions incident to the (100) face of 1.0, 2.5, 5.0, 7.5, and 10.0 kev at target temperatures of 77°K, 20°C, and 200°C.

EXPERIMENTAL TECHNIQUE

A radioactive tracer technique was developed to make the yield and angular distribution measurements. Where long-lived isotopes are involved, this is an extremely desirable technique to employ. It allows for increased sensitivity over a procedure which irradiates and counts the sputtered atoms already on collectors. Mo^{99} has a 66-hour half life, hence one target irradiation provided many sputtering runs.

Maximum snesitivity (cpm/μgm) would be obtained when the target had reached saturation activity. The size of the target prevented irradiation to saturation for health physics reasons. Consequently, the maximum sensitivity was determined by the amount of radiation which could reasonably be handled in the laboratory.

Due to its long half life, the isotope which we chose to trace was Mo^{99}. It has a decay scheme as shown in Figure 1. It will be noticed that there are two decay gammas of appreciably close energy that could be counted by a gamma spectrometer. The spectrometer which was used was not sensitive enough to distinguish between these 0.14 Mev and 0.18 Mev gammas. This resulted in a higher detection sensitivity than if only one of the decay gammas had been counted. It was found that a minimum sensitivity of 30 cpm/μgm of sputtered material yielded acceptable counting statistics.

The target was irradiated in a thermal neutron flux of 1.5×10^{13} neutrons cm^{-2} sec^{-1} for 20 hours. The fast neutron nvt was 1.6×10^{17} neutrons cm^{-2}. Billington and Crawford[5] report a unit cell volume increase of 6.5×10^{-5} percent, and

a change in volume per Frenkel pair of twice the atomic volume. This would then create 6.5×10^{-7} Frenkel pairs per unit cell. This amount of crystal disorder was not enough to affect our measurements. The long irradiation time was necessitated by the low capture cross section of Mo^{98} (26 percent abundant) which would produce the radioactive Mo^{99}.

After the target had been irradiated it was placed in the vacuum system and sputtered. It was found that sensitivities well above the minimum were obtained when a total of approximately 20 millicoulombs of charge was collected by the target. The sputtered atoms were then collected by the collector assembly.

The collector assembly consisted of a square base fabricated from one hundred aluminum cubes (1.1 cm on a side) which were arranged ten on a side. The assembly was placed opposite the target face (see Figure 2) and provided the means for separating the collector so that quantitative angular distribution measurements were possible. After sputtering the target with cesium ions, the cubes were removed and analyzed to determine the radioactivity of each collector, thus providing a relative measure of the amount of molybdenum collected on each cube.

To complete the total yield measurement, the ten-by-ten collector was surrounded with aluminum foil sides and a top foil, thereby enclosing the 2π sterradians below the target. As can be seen from Figure 2, the top foil collector should not directly intercept any sputtered molybdenum. However, for all experiments it collected 3 percent or less of the total

amount. It seems probable that the sticking coefficient was close to one for all but the high energy tail of the sputtered particle energy spectrum and that the 3 percent collected on the top foil can be associated with rebounding of, or resputtering by, the high energy molybdenum from the upper collector face.

The radioactivity of the collector cubes and foils was measured by using a shielded gamma ray spectrometer which discriminates against all background except that associated with the 511 kev positron annihilation gamma radiation. All background that varies in a linear manner with energy in those channels associated with the peak in question was eliminated by computing the number of counts by Covell's method.[6] Absolute measurement of the amount of copper on each collector surface was made by direct comparison with the radioactivity of a known weight of molybdenum irradiated with the target. Hence, the absolute angular distribution throughout a large part of the hemispherical solid angle in front of the target can be directly inferred from the activity of each collector block. The total number of atoms sputtered is clearly computed from the sum of the activity of all collector pieces. The rather laborious process of counting and correcting for radioactive decay with time is circumvented by use of an automatic sample changer with output directly usable for digital computer data reduction.

The total number of ions striking the target was determined by summing and integrating the current to the target and collector assembly which serves as a simplified Faraday cage,

thereby removing any inaccuracy associated with secondary and photoelectron production in the assembly. Auxiliary measurements were made to insure that (a) the ion beam did not strike the collector when entering the assembly, (b) beam divergence after entering was not sufficient to spread the beam to a wider cross sectional area than the target, (c) the ion beam was not contaminated by secondary electrons created in the lens structure by ion bombardment, and (d) negligibly few secondary electrons created at the target could escape the target collector assembly. This last consideration was determined by showing that the summed current was independent of bias voltage between the target and the collector.

DESCRIPTION OF APPARATUS

The equipment used in conducting the experimental portion of the work was designed and constructed by Olson. A detailed description of the apparatus can be found in Reference 4.

The essential pieces of equipment were: a cesium ion source, a transport lens system, a target holder assembly, and a vacuum system which encases all of these parts. A schematic diagram of the equipment is shown in Figure 3.

The cesium ion source contains a reservoir in which a small (one gram) amount of cesium is contained. To create the cesium ions, the reservoir is heated to vaporize the liquid cesium. The vapor then passes through a porous tungsten tip which is maintained at approximately 1200°C. The high temperature is required to maintain a noncesiated tungsten surface. The work function of tungsten (4.5 ev) is greater than the ionizing potential of cesium (3.9 ev). This causes the cesium atoms to be ionized as they pass through the tungsten tip. The singly charged positive ions are drawn away from the tip by the extractor which is held at a potential negative with respect to the tip.

The ion beam is transported to the target via a series of alternating potential lenses and a focusing lens. The focusing lens was not employed in the original system constructed by Olson. It consisted of a large copper disc one-half inch in thickness and two and one-half inches in diameter. There is a three-fourths inch diameter hole in the center through which the beam is allowed to pass. This lens is maintained at a positive potential approximately equal to the potential

applied to the tip. On either side of this focusing lens at a distance of one-fourth inch are lenses, similar to the transport lenses, which are maintained at ground.

The function of the focusing lens was to decrease the beam width at the target to a maximum of three-eights of an inch in diameter. This requirement was necessitated by the small molybdenum target.

Further additions to the original system were in the installation of a cryogenic pump and an ion pump to the target chamber. The cryogenic pump is simply a copper surface of about 1000 cm^2 which has copper tubing attached through which liquid nitrogen flows. The copper surface surrounded three sides of the collector assembly. It is estimated that at 77°K the pumping speed of the cryogenic pump is at least 200 ℓ/s. The addition of the second 200 ℓ/s ion pump brings the total pumping speed in the vacuum chamber to approximately 1000 ℓ/s. The addition of these two pumps decreased the base pressure of the system from 2×10^{-8} torr to $2\text{-}3 \times 10^{-9}$ torr and allowed a pressure of $2\text{-}3 \times 10^{-8}$ torr to be maintained with an ion beam current of about 10 μa on the target.

RESULTS AND DISCUSSION

Sputtering Yield

Sputtering data was recorded for incident ion energies of 1.0, 2.5, 5.0, 7.5, and 10.0 kev. At some of the energies, sputtering was conducted with various target temperatures, i.e., 77°K, 20°C, and 200°C. The sputtering coefficient S (atoms/ion) is shown as a function of incident ion energy and target temperature in Figure 4. Using the results of the work done by Olson and Smith in sputtering copper as a standard of comparision, the molybdenum yield figures agree very nicely with work done previously. Almen and Bruce[7] measured a 45 kev krypton sputtering yield of copper of about 12, whereas Olson and Smith measured a 5 kev cesium-copper yield of about 6.8 atoms/ion. The ratio is 1.77. Almen and Bruce reported a 45 kev krypton-molybdenum sputtering yield of about 3.50, whereas the 5 kev cesium-molybdenum yield measured was 1.8. This ratio is 1.95. A similar comparison can be made between the work conducted by Carlston, Magnuson, Comeaux, and Mahadevan[8] and that reported here. In both cases the data agreed favorably.

As has been shown in prior work by Almen and Bruce,[7] Southern, Willis, and Robinson,[9] and Olson and Smith,[4] alignment of the ion beam with a crystallographic direction can have a marked effect on the yield. Bombarding the target along one of the low indices of the lattice can lead to a low sputtering yield. In the work reported here, alignment was with the $\langle 100 \rangle$ direction (see Appendix A, Target Preparation) with the maximum possible deviation from normal being 3° (half cone angle) due to focusing of the beam by the Einsel lens. Precise

measurements have shown that approximately 80 percent of the beam has a maximum deviation of 1°. Yields under other conditions were not investigated.

The general shape of the yield curves shown in Figure 5 indicate a steady rise in yield with energy. This is not unexpected, for at low energies (below 1.0 kev) the primary mechanism for energy transfer from the ion to the lattice is by ion-atom collisions causing displacements which occur increasingly only in the surface layer as the ion energy is reduced. In this case, sputtering results from a few collisions between atoms initially occupying their appropriate lattice sites. Therefore, one would expect to observe a low yield.

At higher ion energy where a preponderance of sputtering yield data, including that reported here, has been taken, a large fraction of the ion energy is transferred as kinetic energy to the atoms in the surface layers, but the ion does not penetrate much beyond these layers. In this case, a large number of n-body collisions occur throughout the limited volume of the ion-atom and atom-atom interactions. Consequently, many atoms are ejected and the position from which ejection takes place does not correspond to their appropriate geometrical sites. It is in this category that the yield will be a maximum.

The fact that the yield is still increasing with energy indicates that 10 kev cesium sputtering of molybdenum still comes within this region.

Due to the equipment available, sputtering at ion energies above 10 kev was not possible, and the energy of maximum yield

could not be determined. However, when the bombardment ion is at high energy, the energy loss in the surface layers is primarily a result of ionization rather than atomic displacement by ion-atom collisions. Pronounced ion penetration also occurs at these energies, especially when the ion is initially injected parallel to low-index directions. Hence sputtering would occur either as a result of infrequent displacement collisions in the surface layers or when focused momentum chains along close-packed directions (as predicted by Silsbee[3] and simulated by Gibson, et al.[10]) intercept the surface and cause a sputtering event. This assumes that the focusing chains are of a length comparable to the depth of penetration of the ion. As the energy increases, one would then expect increasingly lower yields and increased dependence on focused momentum propagation, with focused ejection more closely parallel to the close-packed direction.

The copper sputtering work done by Olson and Smith indicated this trend of decreasing yield with energy, and there is no reason to suspect that it would not occur in molybdenum at some energy greater than 10 kev.

There is a very evident temperature dependence on the yields shown in Figure 4. To explain this, two considerations must be examined. They are annealing and lattice vibration, both of which are proportional to the temperature.

The annealing of lattice defects caused by ion bombardment has been reported by both Magnuson[8] and Anderson.[11] The temperature at which annealing of the crystal becomes important is not exact. From the data recorded, it would seem that,

within the temperature range investigated, annealing of the molybdenum crystal is occurring.

Near the surface of the crystal there will be a large number of defects (interstitials and vacancies) created during the ion bombardment. These defects will then impair ion penetration deep into the lattice and cause the major portion of energy transfer to occur near the crystal surface. This would tend to increase the sputtering yield. As the temperature is raised, a portion of the defects will be annealed out allowing greater ion penetration. When this occurs, the relative openness of the (100) face shows large unimpeded channels to the bombarding ions. This will then cause energy transfer deeper within the crystal and tend to decrease the yield.

The fact that this effect was not observed in copper can be attributed to the fact that copper will anneal at lower temperatures than will molybdenum. It can be assumed that even at 77°K (lower temperature limit of the measurements made) copper anneals at a rate great enough to mask this temperature dependent yield effect.

Increasing temperature would also decrease the yield by causing the effective length of any focusing chains to be decreased due to the increased lattice vibration.

Angular Distribution

The angular distribution of sputtered particles resulting from ion bombardment parallel to the target surface normal and to the $\langle 100 \rangle$ crystallographic direction should exhibit a fourfold crystal symmetry. Since our data were taken using a

square array symmetrically centered in front of the target surface, we expected and obtained a fourfold degeneracy in the angular distribution independent of the azimuthal orientation of the crystal. The relative angular distribution is presented in tabular form in Tables II and IIA, where the collector positions can be deduced by reference to Figure 5. The value for each position gives the emission per unit solid angle normalized to isotropic emission. In our particular apparatus the solid angle intercepted by the collector blocks varied from 0.065 sr near the normal to 0.018 sr near the edge. As can be seen from Figure 5, the planar angle divergence at a polar angle $\theta = 55°$ (the polar angle of the close packed $\langle 111 \rangle$ direction) is of the order of 10°. Although our angular resolution is essentially equal to the full angular width at half the maximum reported by Molchanov and Tel'kovskii[12] for focused emission in the $\langle 100 \rangle$ direction and is satisfactory for the discussion presented below, the advantage of a finer collection grid is readily apparent. Additional accuracy can be obtained by placing all one hundred collectors in a single quadrant and invoking the symmetry property.

In the report of cesium-copper sputtering by Olson and Smith, it was concluded that close-packed focusing $\langle 110 \rangle$ was not the major contributing factor to the sputtering pattern. It was found that a cosine distribution accounted for more than 75 percent of the emitted particles.[4] Silsbee's criterion for close-packed focusing[3] indicates that molybdenum would focus more readily than copper. Consequently, if focusing chains are

important, they should show a greater contribution in molybdenum than in copper. This was not found to be the case, hence de-emphasizing the importance of focusing chains is not out of order.

A nonlinear regression analysis of the one hundred angular data points, normalized to isotropic emission, was made in order to express the data in analytic form.

$$\frac{2\pi}{S}\frac{dS}{d\Omega}(\theta,\phi) = B_1 \cos^{B_2}\theta \quad \text{where} \quad S = \int_{2\pi} d\Omega(\theta,\phi)\frac{dS}{d\Omega}(\theta,\phi) \qquad (1)$$

B_1 and B_2 were adjusted by the regression analysis to yield the minimum square error between the one hundred data points and the analytic function. The premise upon which Equation (1) is based is that the angular emission from the $\langle 100 \rangle$ bcc lattice under normal bombardment is a peaked cosine distribution centered about the surface normal. The accuracy of the premise can be judged by the 14 percent or less average absolute percent deviation of the one hundred data points (whose accuracy is of the order of 10 percent) from an analytic function which utilized only two fitting parameters. In addition, integration of $dS/d\Omega$, extrapolated over the entire 2π sr in front of the target (see Equation (2) below) predicts a value of the yield that is within 3 percent or less of the measured yield.

$$\frac{4}{S}\int_0^{\pi/2} d\phi \int_0^{\pi/2} d\theta \sin\theta \frac{dS}{d\Omega}(\theta,\phi) = \frac{B_1}{B_2 + 1} \equiv 1 \qquad (2)$$

The results of the nonlinear regression analysis showed very little evidence of ⟨111⟩ close-packed focusing. At the higher energies, 7.5 and 10.0 kev, ⟨111⟩ focusing was noticeable. As in the case of the yield data, measurements will have to be made at higher energies to determine if ⟨111⟩ focusing would become an important consideration.

The curve fitting parameters which gave the best data fit are listed in Table I. It will be noticed that the criterion established for the conservation of particles is fulfilled to within 3 percent for all cases. This is a good indication that the parameters selected do fit the data well. Figure 6 is a plot of the fitting parameter B_2 versus energy. It shows a general increase from the near perfect cosine at low energies to a noticeable peaking at the higher energies. Figure 7 compares the true cosine and that of the largest deviation from the same, i.e., the largest value of parameter B_2.

Molecular beam theory attributes a forward biasing, as has been observed here, to emission from a surface due to source collimation. In the case of the bcc molybdenum crystal focusing from ⟨100⟩ chains would in fact cause preferred ejection in the forward direction. It can then be concluded that ⟨100⟩ focusing due to increased ion penetration is increasing with energy. To further substantiate this, Figure 8 shows the average percent deviation from the selected curve fit of the collectors which correspond to the ⟨100⟩ direction. Again it is seen that the contribution of the ⟨100⟩ points increased with increasing energy. Figure 6 shows the values of the fitting parameter B_2 as a function of both temperature

and energy. If annealing is causing increased ion penetration, then for a given energy, B_2 should increase with increasing temperature showing the increased forward biasing. This is what has been observed. The fact that the forward biasing of the curves seems relatively slight in comparison with the average percent $\langle 100 \rangle$ points is due to the fact that the fitting parameters are determined by equally weighting all one hundred data points, whereas the average percent $\langle 100 \rangle$ deviation considers only those four $\langle 100 \rangle$ points (point 21 in Figure 3).

Another important observation may be made from Figure 8. Examination of the percent deviation for the 77°K curve and the 20°C curve shows that there is a greater percent deviation at the lower temperature. This preferential emission in the $\langle 100 \rangle$ direction indicates that even at the low temperature, when the crystal is most disordered, some of the crystal symmetry is maintained.

SUMMARY AND CONCLUSIONS

Experimental results indicate that sputtering yields of single crystal molybdenum oriented so the ion beam axis is parallel to the $\langle 100 \rangle$ crystal direction are a function of temperature as well as energy. The temperature dependence has been attributed to the fact that with increasing temperature there will be increased annealing allowing greater ion penetration into the crystal. Angular distribution data has supported this. There was a relative increase in sputtering in the forward direction with both increasing energy and increasing temperature. As was in the case of copper sputtering, for the energies and temperatures investigated focusing chains in molybdenum are not an extremely important consideration. Most of the particles were emitted in a cosine distribution which, in this case as well as with copper, can be attributed to atomic ejection from a random lattice.

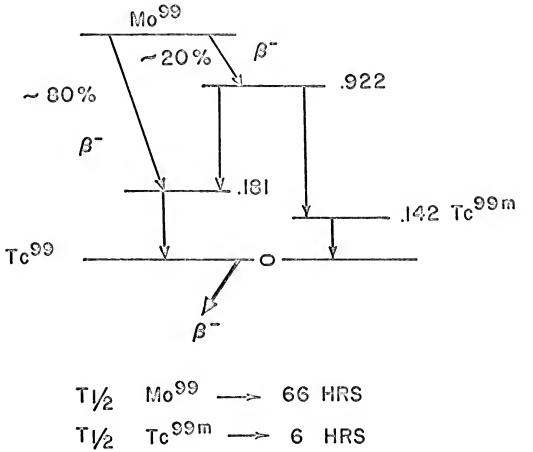

Figure 1. Decay scheme of Mo^{99}.

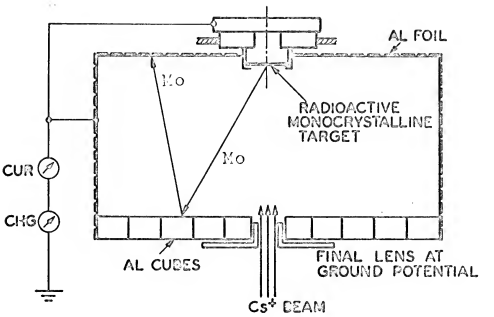

Figure 2. Schematic diagram of target-collector assembly for measurement of the yield and angular distribution of sputtered molybdenum. Secondary sputtering of previously collected molybdenum is depicted.

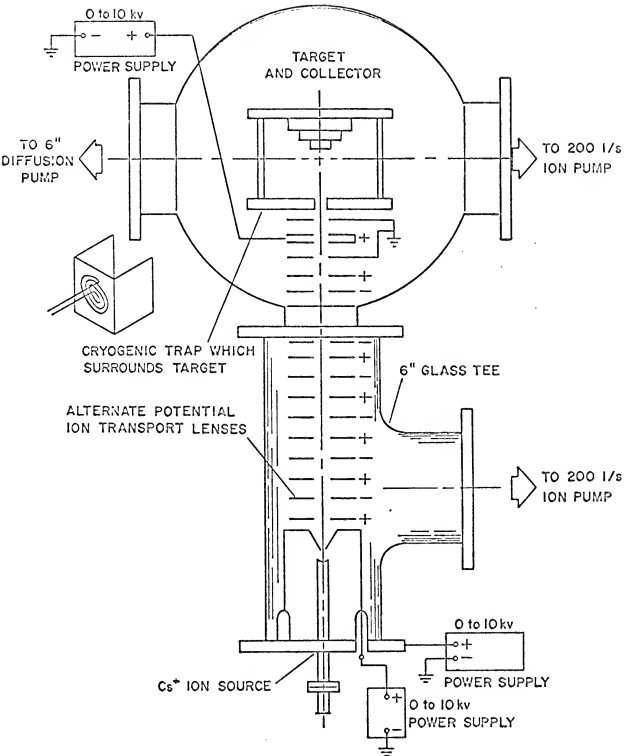

Figure 3

Schematic of the combined ion source and target apparatus.

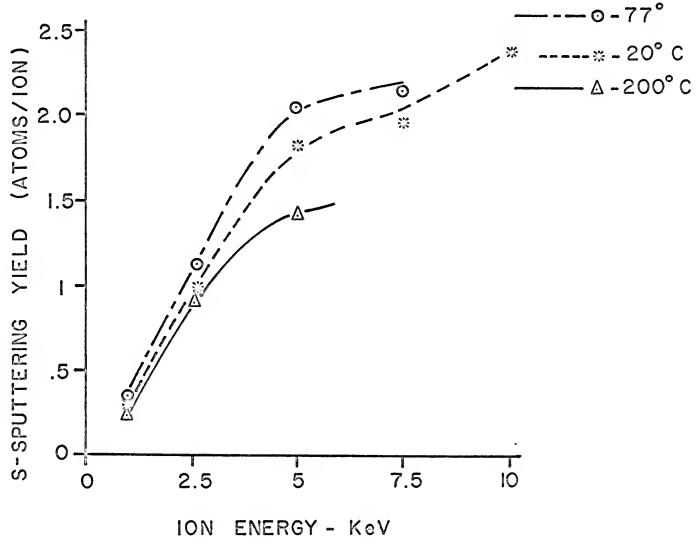

Figure 4. Sputtering yield versus incident ion energy for 1-10 KeV cesium ion bombardment of monocrystalline molybdenum at 77°K, 20°C, and 200°C with the ion beam normal to the surface and parallel to the <100> direction.

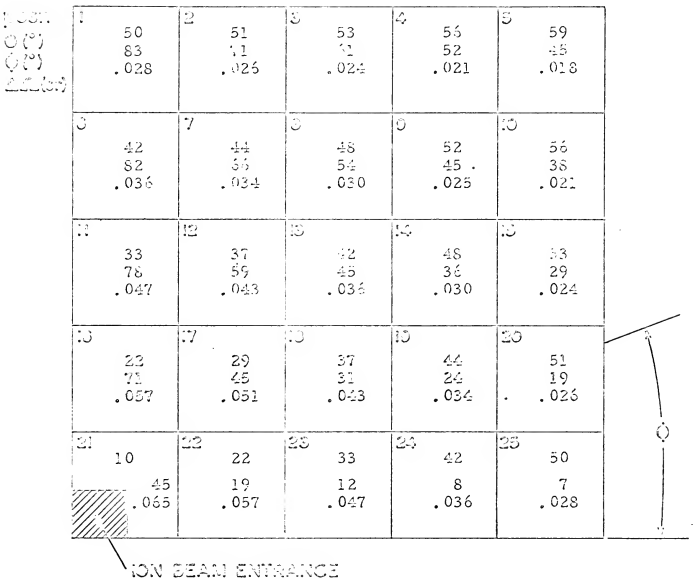

Fig. 5. Schematic diagram of the angular collector positions for normal bombardment of the (100) surface. Θ is the polar angle taken equal to zero along the surface normal while ϕ is the azimuthal angle measured as shown in the surface plane. The solid angle in sterradians is presented for each collector position.

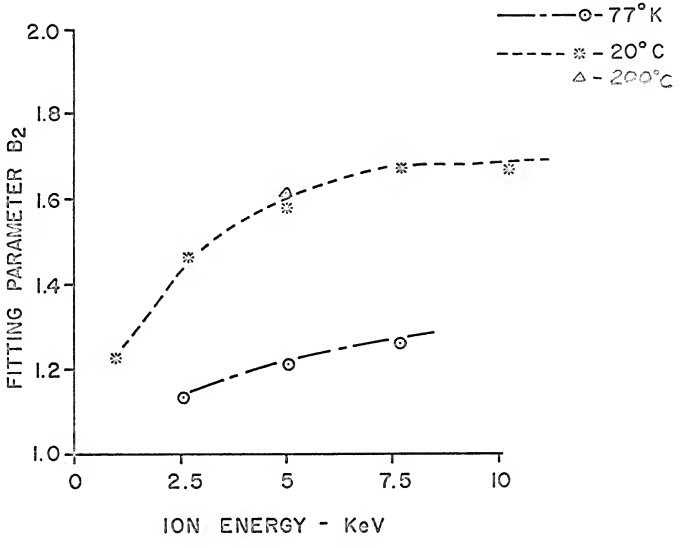

Figure 6. Energy and temperature dependence of fitting parameter B_2.

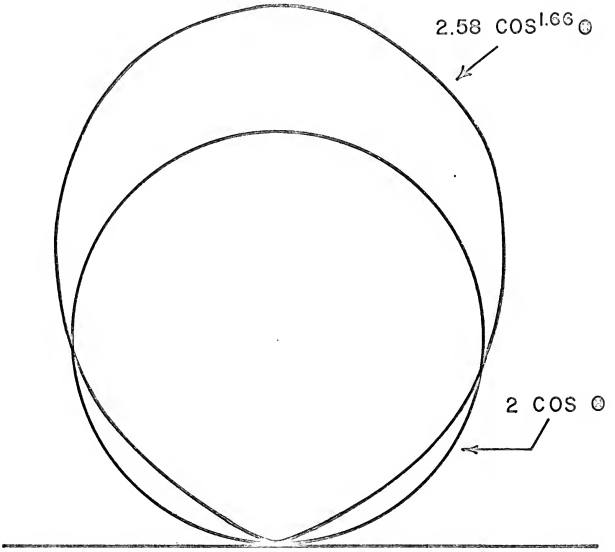

Figure 7. Comparison between polar plot of a true cosine and the curve of the most deviation from the cosine.

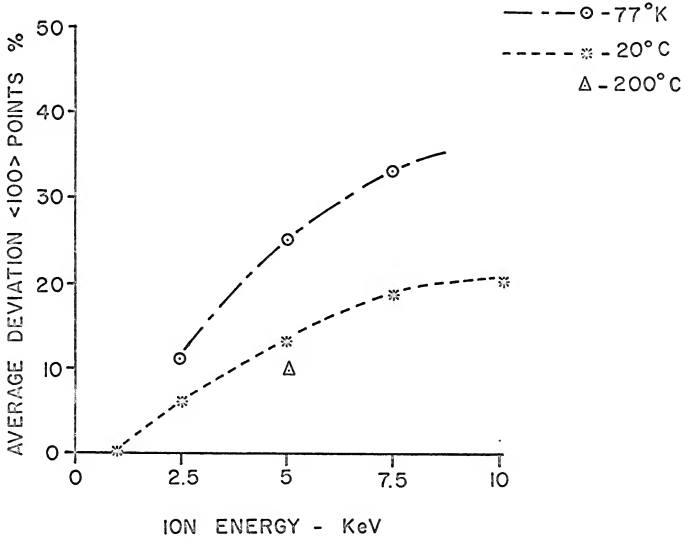

Figure 8. Energy and temperature dependence of the average percent deviation of the four points corresponding to the ⟨100⟩ focusing direction.

ION ENERGY KeV	YIELD	B_1	B_2	$\frac{B_1}{B_2 \div 1}$
1.0*	.35	-	-	-
2.5	1.19	2.18	1.12	1.03
77°K				
5.0	2.05	2.20	1.20	1.00
7.5	2.11	2.20	1.23	0.99

1.0	.26	2.18	1.23	0.98
2.5	0.98	2.51	1.45	1.02
20°C				
5.0	1.78	2.50	1.51	1.00
7.5	1.86	2.58	1.68	0.97
10.0	2.33	2.58	1.66	0.97

1.0*	0.21	-	-	-
2.5*	0.88	-	-	-
200°C				
5.0	1.35	2.56	1.57	1.00

* Angular Distribution Data Not Available

Table I. Yields and fitting parameters B_1 and B_2 as a function of temperature and energy.

ENERGY TEMP.	1.0 KeV 20°C	2.5 KeV 20°C	5.0 KeV 20°C	7.5 KeV 20°C	10.0 KeV 20°C
POSITION			(ΔS/ΔΩ/S/2π)		
1	1.25	1.33	1.31	1.23	1.28
2	1.28	1.33	1.38	1.27	1.28
3	1.15	1.23	1.37	1.25	1.29
4	0.94	1.05	1.22	1.08	1.16
5	0.92	0.93	1.11	0.97	1.12
6	1.55	1.62	1.53	1.51	1.50
7	1.49	1.59	1.46	1.47	1.39
8	1.38	1.46	1.41	1.32	1.34
9	1.19	1.28	1.28	1.18	1.17
10	0.92	0.96	1.00	0.94	0.94
11	1.83	1.93	1.71	1.80	1.79
12	1.77	1.85	1.64	1.69	1.69
13	1.62	1.64	1.53	1.52	1.46
14	1.32	1.38	1.33	1.27	1.21
15	1.12	1.12	1.10	1.04	1.09
16	1.88	2.12	1.98	2.15	2.18
17	1.89	2.03	1.81	1.95	1.97
18	1.76	1.84	1.68	1.73	1.69
19	1.50	1.56	1.43	1.46	1.46
20	1.23	1.26	1.25	1.22	1.23
21	2.02	2.57	2.77	2.94	3.00
22	1.85	2.16	2.06	2.22	2.22
23	1.82	1.93	1.75	1.83	1.87
24	1.59	1.63	1.53	1.55	1.54
25	1.24	1.30	1.27	1.22	1.21

Table II. Normalized relative angular yield data.

ENERGY TEMP.	2.5 KeV 77°K	5.0 KeV 77°K	7.5 KeV 77°K	5.0 KeV 200°C	
POSITION			$(\Delta S/\Delta\Omega/S/2\pi)$		
1	1.35	1.31	1.28	1.29	
2	1.40	1.37	1.34	1.37	
3	1.28	1.43	1.39	1.28	
4	1.19	1.34	1.26	1.08	
5	1.10	1.21	1.14	0.98	
6	1.58	1.41	1.44	1.58	
7	1.52	1.44	1.42	1.52	
8	1.44	1.42	1.40	1.41	
9	1.31	1.32	1.28	1.25	
10	1.02	1.06	1.06	0.99	
11	1.73	1.52	1.60	1.81	
12	1.66	1.46	1.49	1.70	
13	1.55	1.40	1.40	1.56	
14	1.38	1.33	1.29	1.34	
15	1.14	1.10	1.16	1.06	
16	1.94	1.81	1.89	2.05	
17	1.82	1.62	1.68	1.91	
18	1.69	1.50	1.53	1.78	
19	1.51	1.39	1.41	1.51	
20	1.25	1.27	1.23	1.22	
21	2.39	2.76	2.88	2.53	
22	1.93	1.82	1.96	2.03	
23	1.75	1.54	1.61	1.82	
24	1.56	1.44	1.46	1.60	
25	1.31	1.31	1.27	1.26	

Table IIA. Normalized relative angular yield data.

ION ENERGY KeV	AVERAGE % DEVIATION	AVERAGE ABSOLUTE % DEVIATION	RMS DEVIATION
2.5	0.10	6.2	.11
5.0	-0.98	13.7	.25
$77^{\circ}K$			
7.5	0.72	12.5	.24

1.0	-0.38	10.7	.18
2.5	-.08	7.3	.13
5.0	-1.40	12.0	.21
$20^{\circ}C$			
7.5	0.73	11.5	.19
10.0	1.10	10.3	.19

5.0	0.08	10.0	.18
$200^{\circ}C$			

Table III. Average percent deviation, average absolute percent deviation, and RMS deviation as a function of temperature and energy.

APPENDIX A

Target Preparation

Total preparation of the molybdenum target consisted of three distinct procedures. The first step was cutting a small disc from the piece of bar stock available and initial X-ray analysis of the crystal orientation. Following this came the surface preparation by means of electropolishing. The final step was the mounting of the target in its holder and then extensive and precise X-ray analysis by Laue back-reflection to insure proper crystal orientation.

Available was a three inch bar of single crystal molybdenum grown to a diameter of one-half inch by Materials Research Corporation of Orangeburg, New York. The listed impurities were less than 100 ppm. The first X-ray of the crystal showed that the $\langle 100 \rangle$ crystallographic direction was 4° away from the axis of the rod. Knowing this, the next step was to cut a small disc from the rod and have the surface of the crystal perpendicular to the $\langle 100 \rangle$ direction.

In order to obtain a thin disc of the crystal and not inflict any damage to the crystal structure, a spark slicer was employed. The operation of cutting is effected by causing an arc to go from the crystal, which is maintained at approximately 200 volts, to a continuously moving wire at ground potential. The arc would erode the material of the crystal and the wire, hence the reason for having a fresh piece of wire drawn through the cut in the crystal.

The disc cut by the spark cutter was approximately 0.03 of an inch thick. To decrease the size, a spark planer was

employed. The principle of this is exactly identical to that of the spark cutter except that a continuously rotating disc acts as the cathode in place of the wire. This decreased the thickness to 0.02 of an inch. The final reduction of traget size was accomplished by electropolishing.

A primary concern during the target preparation was maintaining as large a surface area as possible. This necessitated coating the edge of the crystal with a nonconducting lacquer during the polishing. The molybdenum crystal served as the anode and a molybdenum rod as the cathode. The electrolyte used was concentrated H_2SO_4 held at room temperature.

It is imperative to operate at the correct current density to insure that polishing occurs and not etching or pitting. The desired operating region is illustrated below:

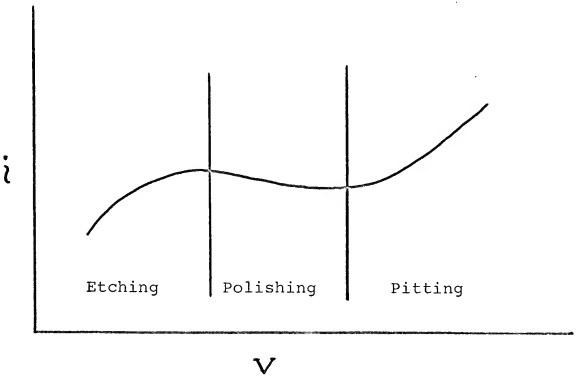

Experimentally it was found that the polishing region varied as a function of time. At the time polishing started, the plateau was reached at an applied voltage of 5 volts. With time, this voltage could be increased to 8 to 10 volts to yield a current density of 0.05 a/cm^2. Polishing was carried out until the target thickness was 0.01 of an inch. The target was then rinsed in distilled water and acetone.

The target was next mounted on its aluminum target holder and extensively X-rayed to insure that the $\langle 100 \rangle$ crystallographic face was perpendicular to the ion beam. The target and holder were then rotated to bring the $\langle 111 \rangle$ crystallographic direction in line with the diagonal of the collector assembly. The accuracy of the crystal orientation is $\pm 1°$.

APPENDIX B

Covell Method and Computer Data Reduction Program

B.1. Covell Method: The amount of molybdenum on each of the aluminum collectors was measured by comparing the activity on each collector with the activity of a known weight (or standard) of molybdenum. The individual collectors and the standard were analyzed with a multi-channel analyzer for a preset length of time. The amount of activity on the collectors and standard was then proportional to the area under the 0.511 Mev annihilation photopeak of Mo^{99}. To determine this area, the method of Covell[6] was used.

Taking advantage of the digital nature of the output from the pulse height analyzer, Covell considered the area under the photopeak to be represented by the area above the line connecting the n^{th} channel either on either side of the peak channel rather than drawing a horizontal line through the photopeak. This is illustrated in Figure 9. The peak channel is designated by the index zero and has an amplitude of a_o, while the n channels above and below a_o have amplitudes b_1, b_2, . . . , b_n and a_1, a_2, . . . , a_n, respectively.

Covell's method has the advantage that it is readily adaptable to digital computer analysis, and it also eliminates constant background contributions to the area under the photopeak. If P represents the total area under the photopeak, N is given by

$$N = P - Q \qquad \text{(B-1)}$$

From Figure 9 it is apparent that

$$P = a_o + \sum_{i=1}^{n} a_i = \sum_{i=1}^{n} b_i \qquad \text{(B-2)}$$

and

$$Q = a_n(n + n + 1) + 1/2(2n + 1)(b_n - a_n)$$

$$= (n + 1/2)(a_n + b_n) \qquad \text{(B-3)}$$

Substituting Equations B-2 and B-3 into B-1 gives for N

$$N = a_o + \sum_{i=1}^{n} a_i + \sum_{i=1}^{n} b_n - (n + 1/2)(a_n + b_n) \qquad \text{(B-4)}$$

Since N is representative of a radioactive decay process, it is possible to assign a standard deviation to it. Equation B-4 is the algebraic sum of 2N + 1 independent terms, each of which may be considered to have a Poission distribution. The estimated variance of the number of counts may be written as

$$S^2(N) = a_o + \sum_{i=1}^{n} a_i + \sum_{i=1}^{n} b_i + [(n - 1/2)^2](a_n + b_n) \qquad \text{(B-5)}$$

which can be simplified to

$$S^2(N) = N + (n + 1/2)(n - 1/2)(a_n + b_n) \qquad \text{(B-6)}$$

from this expression the standard error is

$$S(N) = \sqrt{N = (n + 1/2)(n - 1/2)(a_n + b_n)} \qquad (B\text{-}7)$$

B.2. Computer Data Reduction Program: Using the above method developed by Covell, a computer program was written adapting Equation B-4 and B-7 for calculating the amount of molybdenum on the individual collectors. The multi-channel analyzer output which was punched onto paper tape was converted to computer punch cards. With data in this form, the data reduction using Equations B-4 and B-7 was easily adapted to a digital computer.

The sequence of analysis of the aluminum collector blocks and foils was such that samples 1 to 100 were the aluminum blocks (see Figure 5 for numbering sequence), samples 101 and 102 were the aluminum foil sides (two sides per sample), sample 103 was the top foil collector and sample 104 was the standard mass. The photopeak area associated with each sample was calculated from Equation B-4 and was identified by COUNT(j) in the program where j varied from 1 to 104.

The usual CTIMEC was either 5 or 6 minutes, so that the total analysis time per sample (DTIME) was 5.80 or 6.80 minutes and for 103 samples (1-103) the time difference between analysis of the first and last samples was 10 to 12 hours. The activity of the Mo^{99} standard (104) was too great to be counted immediately, consequently it was allowed to decay for a time designated WTIME. Since the Mo^{99} half-life is 66 hours, it was necessary to correct for the decay in the intensity of the individual collectors. This correction was accomplished by multiplying all COUNT(j) by the factor

$$EXPL(j) = e^{\lambda(j-1)DTIME} \tag{B-8}$$

$$EXPL(104) = e^{\lambda WTIME} \tag{B-8a}$$

This corrected all of the COUNT(j) values back to time t = 0. The photopeak areas which were corrected for the decay suffered were called CCOUNT(j) and were given by

$$CCOUNT(j) = COUNT(j)EXPL(j) \tag{B-9}$$

Similarly, the standard deviation was calculated using Equation B-7 and was called SIGMA(j) and the time corrected quantity was called CSIGMA(j).

The actual weight of molybdenum on each collector was then easily calculated by the following relation

$$(molybdenumweight)j = (Std.Weight) * \frac{N_j}{N_{104}} * \frac{(Count\ Time)_j}{(Count\ Time)_{104}} \tag{B-10}$$

or in terms of computer language

$$AMASS(j) = STDMAS * \frac{CCOUNT(j)}{CCOUNT(104)} * \frac{CTIMEC}{CTIMES} \tag{B-11}$$

From the quantity AMASS(j) the total amount of molybdenum sputtered and the total yield were easily calculated. The total amount of molybdenum sputtered is

$$\text{MOMASS} = \sum_{j=1}^{103} \text{AMASS}(j) \qquad \text{(B-12)}$$

and the total yield, in atoms ejected per incident ion, is

$$\text{YIELD} = \frac{\text{MOMASS} * \text{APMG}}{\text{CSIONS}} \qquad \text{(B-13)}$$

where APMG equals the number of atoms per milligram and CSIONS = CHARGE/1.602 x 10^{-19}.

The angular distribution of the sputtered molybdenum was calculated by dividing the amount of molybdenum on each collector by the solid angle that the collector subtends with respect to the target. This quantity would be expressed by

$$\left(\frac{\Delta S}{\Delta \Omega}\right)_j$$

However, this ratio was normalized by dividing by $S/2\pi$. Thus, the normalized yield per unit solid angle was calculated by

$$\text{PYPSA}(j) = \frac{\text{AMASS}(j)}{\text{MOMASS}} * \text{TPODO}(j)$$

where TPODO(j) is the factor $2\pi/\Delta\Omega_j$. The $\Delta\Omega_j$ had to be calculated for each collector so that TPODO(j) was an input parameter in the program.

Based on this outline of the computer data reduction program, the FORTRAN IV source program is:

Input Parameters

1) L = Number of channels above and below channel of maximum

2) DEKCON = Decay constant of isotope being used. Units = min^{-1}

3) DTIME = Time difference between beginning of each sample count. Units = min

4) CTIMEC = Amount of time collectors are counted. Units = min

5) CTIMES = Amount of time standard is counted. Units = min

6) STDMAS = Mass of standard. Units = milligrams

7) APMG = Number of atoms per milligram of the material being investigated

8) CHARGE = Total charge collected on target. Units = coulombs

9) WTIME = Time difference between starting count times of standard (104) and sample (1)

10) TPODO(j) = $2\pi/\Delta\Omega_j$ = solid angle and normalization factor for the j^{th} collector

Fortran Program

```
C       ANGULAR YIELD DISTRIBUTION
        DIMENSION N(104,104), NSUM(104),COUNT(104), SIGMA(104),
       XCCOUNT(104), CSIGMA(104), DEV(104), AMASS(104), ABN(104)
       XPERC(104),DPERC(104),PYPSA(100),TPODO(100),EXPL(104)
     1 READ99,(TPODO(J),J=1,100)
     2 READ100,L,DEKCON,DTIME,CTIMEC,CTIMES,STDMAS,APMG,CHARGE,
           WTIME
     3 READ101,((N(I,J),I=1,104),J=1,104)
C
        CSIONS=CHARGE/1.602E-19
        AKON=DEKCON*DTIME
        PLUS=FLOAT(L)+0.5
        PROD=PLUS*(FLOAT(L)-0.5)
C
     5  IO=5
     6  DO 8 I=6,104
        IF (N(I,104)-N(IO,104))8,8,7
     7  IO=I
     8  CONTINUE
        IMAX=IO
C
     9  DO 12 J=1,103
        NSUM(J)=N(IO,J)
    10  DO LL K=1,L
        KH=IO+K
        KL=IO-K
    11  NSUM(J) = NSUM(J) + N(KH,J + N(KL,J)
        IH=IO+L
        IL=IO-L
        ABN(J)=FLOAT(N(IL,J) + N(IH,J))
        COUNT(J)=FLOAT(NSUM(J))-PLUS*ABN(J)
        SIGMA(J)=SQRT(COUNT(J)+PROD*ABN(J))
        EXPL(J)=EXP(AKON*FLOAT(J-1))
        CCOUNT(J)=COUNT(J)*EXPL(J)
    12  CSIGMA(J)=SIGMA(J)*SQRT(EXPL(J))
        NSUM(104)=N(IO,104)
    13  DO 14 K=1,L
        KH=IO+K
        KL=IO-K
    14  NSUM(104)=NSUM(104)+N(KH,104)+N(KL,104)
        IH=IO+L
        IL=IO-L
        ABN(104)=FLOAT(N(IL,104)+N(IH,104))
        COUNT(104)=FLOAT(NSUM(104))-PLUS*ABN(104)
        EXPL(104)=EXP(DEKCON*WTIME)
        CCOUNT(104)=COUNT(104)*EXPL(104)
    15  RATIO=(CTIMES*STDMAS)/(CCOUNT(104)*CTIMEC)
        AMASS(104)=STDMAS
        DEV(104)=(STDMAS*CSIGMA(104))/CCOUNT(104)
```

```
   16 DO 17 J=1,103
      AMASS(J)=CCOUNT(J)*RATIO
   17 DEV(J)=CSIGMA(J)*RATIO
C
      MOMASS=0
   18 DO 19 J=1,103
   19 MOMASS=MOMASS+AMASS(J)
      YIELD=(APMG*MOMASS)/CSIONS
C
   20 DO 21 J=1,103
      PERC(J)=AMASS(J)/MOMASS
   21 DPERC(J)=DEV(J)MOMASS
      TDEV=0
   22 DO 23 J=1,103
   23 TDEV=DEV(J)**2 + TDEV
      TDEV=SQRT(TDEV)
      DYIELD = (APMG*TDEV)/CSIONS
   24 DO 25 J=1,100
   25 PYPSA(J) = PERC(J)*FLOAT(TPODO(J))
C
   40 PRINT 500
   41 PRINT 200, CHARGE
   42 PRINT 201,IMAX
   43 PRINT 501
   44 PRINT 202
   45 PRINT 203. (J,AMASS(J),DEV(J),PERC(J),DPERC(J),PYPSA(J),
          J=1,104)
   46 PRINT 204,MOMASS
   47 PRINT 205,TDEV
   48 PRINT 206,YIELD
   49 PRINT 207,DYIELD
      STOP
C
   99 FORMAT (l814)
  100 FORMAT (I2,E9.2,F5.2,2F5.1,F5.2,3E9.2)
  101 FORMAT (I6,7I10)
  200 FORMAT (16H TOTAL CHARGE = ,E12.3)
  201 FORMAT (22H CHANNEL OF MAXIMUM = , 13)
  202 FORMAT (66H    J     AMASS(J)      DEV(J)    PERC(J)   DPERC(J)
     X    PYPAS(J)/)
  203 FORMAT (l5,4E12.3,E13.3)
  500 FORMAT (lH1)
  501 FORMAT (///)
  204 FORMAT (//16H         CUMASS=,E12.3)
  205 FORMAT (//16H           TDEV=,E12.3)
  206 FORMAT (//16H          YIELD=,E12.3)
  207 FORMAT (//16H         DYIELD=,E12.3)
      END
```

Output

The program instructs the computer to print out the following information:

1) CHARGE = Input quantity charge for identification

2) IMAX = Channel number of greatest intensity for sample 104 (STDMAS)

3) AMASS(j) = Molybdenum mass on j^{th} collector. Units = milligrams

4) DEV(j) = Standard deviation of mass on j^{th} collector. Units = milligrams

5) PERC(j) = Percent of total mass sputtered on the j^{th} collector

$$= \text{AMASS(j)} / \sum_{j=1}^{103} \text{AMASS(j)}$$

6) DPERC(j) = Standard deviation of percent on j^{th} collector

7) PYPSA(j) = $\left(\frac{\Delta S}{\Delta \Omega}\right)_j / \frac{S}{2\pi}$

8) MOMASS = Total amount of molybdenum sputtered

$$= \sum_{j=1}^{103} \text{AMASS(j)}.$$ Units = milligrams

9) TDEV = Standard deviation of MOMASS

10) YIELD = Number of atoms ejected per incident ion

11) DYIELD = Standard deviation of YIELD.

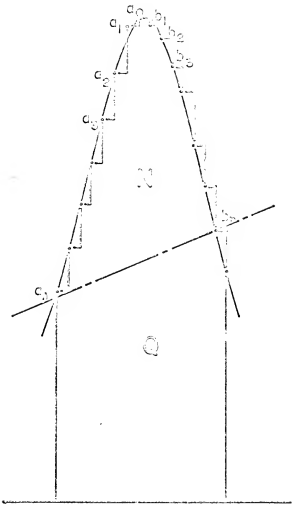

Figure 9. Covell method for determining area under photopeak.

REFERENCES

1. Grove, Phil. Trans., (1852).
2. Wehner, G., Advances in Electronics and Electron Physics 7, 239 (1955).
3. Silsbee, R. H., J. Appl. Phys. 28, 1246 (1957).
4. Olson, N. T., Angular Distribution and Yield Measurements of Single Crystal Copper Sputtered by 1 to 10 kev Cesium Ions, Ph.D. Thesis, Department of Nuclear Engineering, University of California, Berkeley, California, 1966.
5. Billington, D. S., and Crawford, J. H., Jr., Radiation Damage in Solids, Princeton University Press, Princeton, N. J., 1961, pp. 101-102.
6. Covell, D., U. S. Daval Radiological Defense Laboratory, Hunters Point, California, USNRDL-TR-288.
7. Almen, O., and G. Bruce, Nucl. Instr. and Meth. 11, 257 (1961).
8. Carlston, C.E., G. D. Magnuson, A. Comeaux, and P. Mahadevan, Phys. Rev. 138 A759 (1965).
9. Southern, A., W. Willis, and M. Robinson, J. Appl. Phys. 34, 153 (1963).
10. Gibson, J., A. Goland, M. Milgram, and G. Vineyard, Phys. Rev. 120, 1229 (1960).
11. Anderson, G. S., G. K. Wehner, and H. J. Olin, J. Appl. Phys. 34, 3492 (1963).
12. Molchanov, V. A., and Tel'kovskii, V. G., Bull. Acad. Sci. USSR, Phys. Ser. (USA) 26, 1470-1476 (1963).